



Mapping of Iron Oxide Distribution on the Ground Surface of the Tugu Barat Oil and Gas Field Using Landsat 8 OLI and Field Data

Tri Muji Susantoro¹, Suliantara¹, Ketut Wikantika², Asep Saepuloh³, Agung Budi Harto², Herru Lastiadi Setiawan¹, Fitriani Agustin⁴, Adis Jayati⁵, Kurdianto¹, Sayidah Sulma⁶ and Sukristiyanti⁷

¹Research Center for Geoinformatics, National Research and Innovation Agency
Jakarta-Bogor Street Km. 46, Cibinong, Bogor Regency, West Java 16911, Indonesia.

²Department of Geodesy and Geomatics, Bandung Institute of Technology
Ganesa Street No.10, Lb. Siliwangi, Coblong District, Bandung City, West Java 40132, Indonesia.

³Department of Geology–Bandung Institute of Technology
Ganesa Street No.10, Lb. Siliwangi, Coblong District, Bandung City, West Java 40132, Indonesia.

⁴Center for Geological Survey, Ministry of Energy and Mineral Resources
Diponegoro Street 57, Bandung 40122, Indonesia.

⁵Directorate of Laboratory Management, Research Facilities and Science and Technology Areas – National Research and Innovation Agency, Gatot Subroto Street No.10, Mampang Prapatan, South Jakarta, 12710, Indonesia

⁶Research Center for Oceanography–National Research and Innovation Agency, Gatot Subroto Street No.10, Mampang Prapatan, South Jakarta, 12710, Indonesia.

⁷Research Center for Geological Disaster–National Research and Innovation Agency, Gatot Subroto Street No.10, Mampang Prapatan, South Jakarta, 12710, Indonesia.

Corresponding author: trim010@brin.go.id.

Manuscript received: July 02th, 2024; Revised: July 31th, 2024
Approved: August 07th, 2024; Available online: December 02th, 2024.

ABSTRACT - Previous studies have demonstrated that Landsat series data can be utilized to map rock change in arid and semi-arid environments. In this study, Landsat 8 Operational Land Imager (OLI) was used to map the presence of iron oxide (ferrous, ferric, and hematite) in the topsoil of the Tugu Barat Oil and Gas Field, Northwest Java Basin, Indonesia. The aim is to map the distribution of iron oxide and analyze it for detection of the presence of microseepage. The results show that the concentration of the mineral hematite indicates an anomaly, where the edge of the field is very low and tends to rise in the middle, but this condition is unclear, because of the presence of red soil containing high hematite in the north. Based on analysis indicates an anomaly, where the edge of the field is very low and tends to rise in the middle, but this condition is unclear, because of the presence of red soil containing high hematite in the north. Based on analysis of Landsat 8 OLI data, ferrous oxide concentrations show an increase at the edge of the field, especially in the southeast. However, this condition is less visible in the west because of the high vegetation density. The ferric oxide concentration shows the opposite pattern to the ferrous oxide concentration. These results are supported by the ferrous oxide index results from soil reflectance spectra recorded using Analytical Spectral Devices (ASD). Where the ferrous oxide concentration is low at the edge then tends to rise in the middle of the field. Meanwhile, the analysis of ferric oxide from the spectral reflectance of soil from ASD results does not show clear differences. The Normalized Iron Oxide Difference Index (NIODI) analysis shows the presence of small amounts of hematite and no goetite. The research results show evidence of microseepage indications at the edge of the field, especially at the southeastern edge. Iron oxide mapping has

the potential to support oil and gas exploration through analysis of alteration processes which are thought to be the impact of micro-seepage.

Keywords: iron oxide, soil spectral, hematite, NIODI, landsat 8 OLI.

© SCOG - 2024

How to cite this article:

Tri Muji Susantoro, Suliantara, Ketut Wikantika, Asep Saepuloh, Agung Budi Harto, Herru Lastiadi Setiawan, Fitriani Agustin, Adis Jayati, Kurdianto, Sayidah Sulma and Sukristiyanti, 2024, Mapping Iron Oxide Distribution on the Ground Surface of the Tugu Barat Oil and Gas Field Using Landsat 8 OLI and Field Data, *Scientific Contributions Oil and Gas*, 47 (3) pp. 189-203. DOI. org/10.29017/SCOG.47.3.1634.

INTRODUCTION

Iron oxides are the second most common mineral group found in hydrothermally altered rocks. Ouattara et al. (2004) explain remote sensing for iron oxides through their research at White Mountain, Beaver County, Utah, USA, utilizing a Landsat TM band 3 to 1 ratio. The findings indicate that locations with significant iron oxide seem brighter. This is because iron oxide absorbs blue wavelengths, resulting in minimal reflection, whereas red wavelengths produce strong reflection. Rocks with ferromagnetic minerals absorb light at around 1.0 μm (Hunt et al. 1974; Hunt & Salisbury 1976).

Landsat series data have been effectively used to detect altered rocks in dry and semi-arid environments. However, in tropical areas, mapping of altered rocks sometimes experiences limitations due to high vegetation density (Rajesh 2004). Oil and gas seepage causes an increase in ferrous minerals and a decrease in ferric minerals as a result of the oxidation-reduction process (Hong 1999). It can support oil and gas exploration through surface anomaly studies (Susantoro et al. 2023a). Although detecting mineral alteration in densely vegetated areas can be challenging (Suliantara et al. 2021), it is still possible to recognize them based on differences in topographic anomaly (Cristiana et al. 2015, 2014).

In Advanced Spaceborne Thermal Emission and Reflection Radiometer (ASTER), the band ratio of 2 to 1 sharpens the iron oxide and differentiates the iron oxide zone. The influence of hydrocarbons will reduce environmental conditions by transforming sulfate ions into sulfide ions which results in the reduction of hematite to pyrite. The hydrogen atoms released from this reaction will react with the existing feldspars resulting in kaolinite precipitation. This condition favors the reaction between bicarbonate

ions and Ca ions which causes the deposition of calcite in the open pores after the reduction and removal of hematite (Petrovic et al. 2012). The iron oxide phase reflects the pH, redox potential, humidity, and temperature conditions in the soil environment. The presence of iron oxide can be reflected in the color of the soil. Remote sensing can be used to detect the presence of iron oxide based on visible-near infrared wavelength reflection (Viscarra Rossel et al. 2010).

Analysis of the presence of iron oxide can be done by comparing the wavelength of 0.63 - 0.69 μm (band 3) with 0.45 - 0.52 μm (band 1) on Landsat 7. The results of this comparison depict the zone of hematitic changes (Ouattara et al. 2004). Carbon dioxide in the soil layer, in the form of carbonic acid, can react with clay minerals, resulting in secondary calcium carbonate precipitation and silicification. In acidic circumstances, bacteria process and create hydrocarbon oxidation, diagenetic weathering of feldspar into clay, leaching of potassium and radioactive elements from clay, and conversion of smectite to iron carbonate, also known as delta carbon. Delta C conditions in oil and gas structures are high at the edge of oil and gas accumulation (Salati 2014). In oil and gas fields, the interaction of hydrogen sulfide with iron oxide can result in magnetite, maghemite, pyrrhotite, and greigite anomalies. However, these anomalies sometimes occur due to an increase in the magnetic ratio in the ground, which can be related to rainfall and climate (Liu et al. 1994; Maher & Thompson 1992).

In this study, mapping of the distribution of iron oxide in topsoil in the Tugu Barat oil and gas field, Northwest Java Basin, Indonesia was carried out using Landsat 8 Operational Land Imager (OLI) and supported by field survey data. The Tugu Barat oil and

gas field has been proven to have geomorphological anomalies characterized by a low wetness index and coarser sediment distribution at the peak anticline than at its flanks. (Susantoro et al. 2023b). Apart from that, there are also clay mineral anomalies that indicate the presence of microseepage on the surface (Susantoro et al. 2020), and plants experience stress at the edge of the anticline structure (Susantoro et al. 2024). Based on this, research was carried out to map the distribution of iron oxide within this oil and gas field, and analyze it to detect the presence of micro seepage.

METHODOLOGY

Study Location, Data and Processing

The study location is an oil and gas field in the border area of Indramayu and Majalengka (Figure 1). At this location, it is indicated that there is a micro-seepage which is characterized by vegetation stress (Susantoro et al., 2019, 2018), the presence of clay mineral anomalies (Susantoro et al. 2020), and oil and gas leaks around the wellhead.

The data used is Landsat 8 OLI with path/row121/065 which was downloaded from the

website <https://earthexplorer.usgs.gov/>. The data was acquired on September 25, 2015. The initial steps in this study include pre-processing which starts with atmospheric correction and continues with geometric correction. The results show the root mean square error (RMSE) is 0.3 pixels.

The next process is the analysis of the iron oxide index which is formulated according to Formula 1 (Drury 1987) and Formula 2 (Shi et al. 2010).

$$\text{Ferric oxide index} = \frac{\text{Red}}{\text{Blue}} \quad (1)$$

$$\text{Ferrous oxide index} = \frac{\text{SWIR}}{\text{NIR}} \quad (2)$$

where, Red = Red band with a wavelength of 0.63 - 0.69 μm ; Blue = Blue band with a wavelength of 0.45 - 0.52 μm ; SWIR = Shortwave-infrared with a wavelength of 1.55 - 1.75 μm ; and NIR = Near-infrared with a wavelength of 0.76 - 0.90 μm .

It is hoped that this band ratio can assess changes in ferric and ferrous oxide concentrations in oil and gas fields. It is suspected that in the oil and gas field, there will be an increase in ferrous minerals and a decrease in ferric.

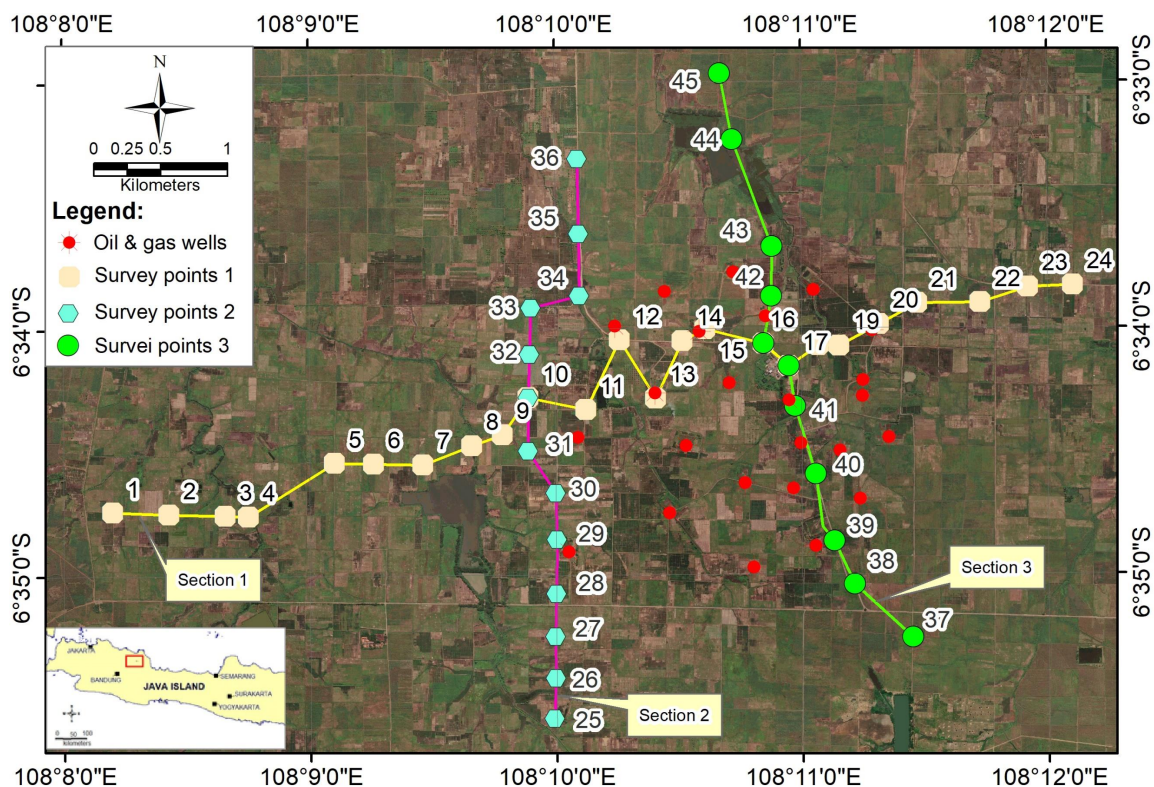


Figure 1

Coverage of the research area and plot of soil sampling locations and spectral measurements for hematite analysis.

The names ferric and ferrous indicate differences in the complexity of the Fe content. The Latin name for iron is ferrum, therefore the difference in the endings in ferrous and ferric indicates the oxidation state of the iron ion in the compound. Ferrous is an iron atom that loses two electrons to form Fe+2 or written Fe(II), while ferric is an iron atom that loses three electrons to form Fe+3 or written Fe(III). Ferrous Oxide is a compound of iron which when it reacts with oxygen in the air will produce black iron oxide which is also called the mineral wustite, while Ferric Oxide is iron which when it reacts with oxygen produces reddish iron oxide or what is known as the mineral hematite and rust (Bergstresser 2018).

Field Survey

Field surveys were carried out to record soil spectra and soil samples to be sent to the sediment laboratory for identification of hematite compounds. Soil spectral recording was carried out using a hyperspectral ASD which produces 2151 bands at a wavelength of 350 – 2500 nanometers (Figure 2). Meanwhile, identification of hematite compounds was carried out by soil sampling and then analysis was carried out using XRD. This survey was carried out at 45 locations in the North-South and West-East directions across the Tugu Barat oil and gas field.

Analysis

The analysis carried out includes: (1) resampling spectral reflectance measurements with ASD to Landsat 8 OLI spectral measurements. (2) Analysis of the iron oxide index (formulas 1 and 2), and the Normalized Iron Oxide Difference Index (NIODI) (Viscarra Rossel et al. 2010) even though Fe oxides play an important role in soil function. Fe oxides reflect the conditions of pH, redox potential, moisture, and temperature in the soil environment. The strong pigmenting effect of Fe oxides gives most soils their color, which is largely a reflection of the soil’s Fe mineralogy. Visible–near-infrared (vis–NIR, using formula 3. The NIODI is used to differentiate the presence of hematite and goethite based on spectral reflectance recorded using ASD. (3) carry out descriptive analysis to identify the presence of iron oxide anomalies in oil and gas fields. (4) regression analysis to examine the relationship between hematite content and spectral reflectance.

$$NIODI = \frac{(D920 - D880)}{(D880 + D920)} \tag{3}$$

where D880 and D920 are the radian values at wavelengths of 0.88 μm and 0.92 μm. NIODI values range from -1 to 1 with positive indicating the

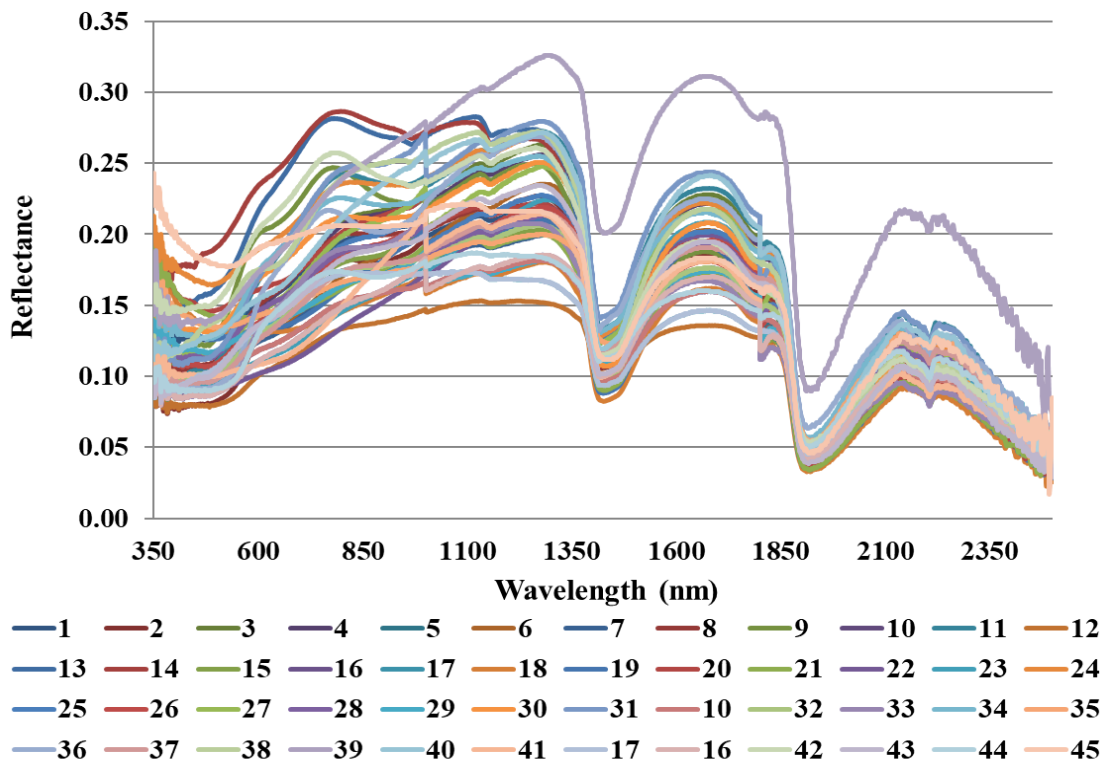


Figure 2
Reflectance of soil, recorded using ASD.

presence of goethite and negative values indicating the presence of hematite. Values close to zero or zero indicate increased uncertainty or the presence of both goethite and hematite. NIODI values generally indicate the relative ratio of goethite to hematite without any precise estimate of the amount in the soil.

RESULT AND DISCUSSION

Hematite Mineral Composition

The results of the hematite concentration analysis in Tugu Barat are depicted in Table 1. The hematite concentration in track 1 shows a small-scale anomaly, where it was not found at the edge of the oil and gas field but in the middle, it was found with a content of around 4% (Figure 3a). On Track 2, the hematite content increases to the north then decreases at the edge of the oil and gas field and rises again outside the field (Figure 3b). The highest hematite concentration is outside the oil and gas field, namely in the north with a value of 10%. In track 3, the hematite concentration is very low in the south of the field, then increases in the middle of the oil and gas field, decreases at the edges, and increases again outside the field (Figure 3c). Field survey data noted that the location with the highest hematite concentration was red soil. This physically indicates that it contains high levels of iron oxide. Hematite is a red iron mineral that is found in large quantities in rocks and soil. (Hidayat et al. 2002)

explained that iron oxide greatly influences available water and the plasticity index. The higher the iron oxide, the higher the available water, the lower the plasticity index, the easier the soil to use, and the redder the color. However, in small concentrations iron oxide in the soil can affect the color of the soil to red (Schwertmann & Taylor 1989).

The formation of iron oxide occurs due to the oxidation reaction of pyrite in acid sulfate soil which produces goethite and hematite. Goethite will gradually change to hematite in further oxidation reactions (Annisa & Purwanto 2010). Oxidation and reduction reactions are common occurrences along migration routes and in areas affected by microseepage (Shi et al. 2010). The distribution map of the percentage of hematite mineral concentration is in Figure 4, while the hematite distribution graph for each cross-section can be seen in Figure 3.

Iron Oxide Index on Landsat 8 OLI

The ferrous oxide index results at the study location ranged from 0.115 - 2.00, with the dominant ferrous oxide index value ranging from 0.21 - 1.96 and with an average of 1.019. Specifically at the study location, namely around oil and gas fields, the ferrous oxide index ranges from 0.21 – 1.96.

The mapping results show that the area thought to be a microseepage based on the ferrous iron oxide index has increased compared to the surrounding

Survey Point	Hematit (%)	Survey Point	Hematite (%)	Survey Point	Hematite (%)
1	0	16	3	31	0
2	4	17	1	32	2
3	0	18	0	33	5
4	0	19	0	34	6
5	0	20	0	35	2
6	0	21	0	36	10
7	0	22	0	37	0
8	0	23	0	38	0
9	2	24	0	39	2
10	1	25	0	40	0
11	1	26	0	41	0
12	4	27	0	42	2
13	4	28	0	43	0
14	2	29	0	44	10
15	2	30	0	45	0

Table 1
The hematite concentration is based on XRD analysis.

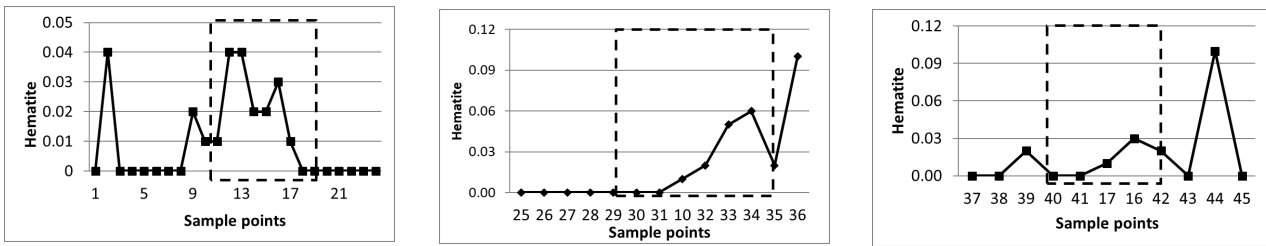


Figure 3

Graph of the distribution of hematite minerals in 3 survey tracks, (a) Survey Track 1, (b) Survey Track 2, and (c) Survey Track 3.

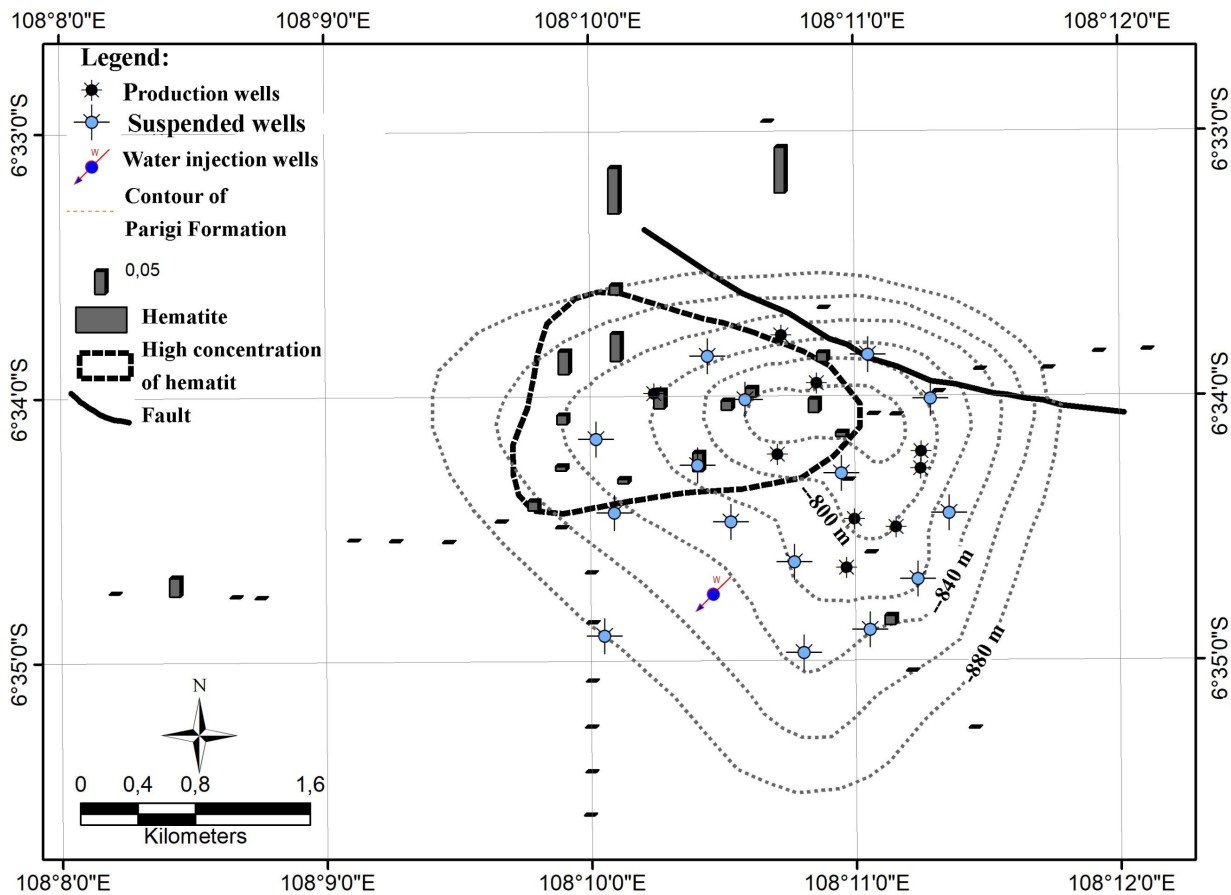


Figure 4

Map of distribution of the percentage of hematite mineral concentration on 3 survey tracks at the study location.

area. The increase in the value of field edge ferrous oxide occurs due to oil and gas accumulation as a result of acidic conditions which are the result of hydrocarbon oxidation (Saunders et al. 1999; Schumacher 1996).

Analysis of the ferrous oxide index from Landsat 8 OLI at 45 sample points shows that there are changes in values in the oil and gas field. In general, in oil and gas fields there is an increase in the ferrous oxide index value. On track 1 outside the oil and gas field to the west, the ferrous oxide index value

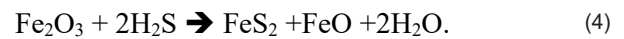
is low with a value of 0.80, then rises gradually to 1.52 and falls again in the middle of the field. The ferrous oxide index value then rose again to approach the eastern edge of the field with an index value of 1.41. Then towards the outside of the oil and gas field, the index value drops to 1.00 and then rises again towards the outside of the field (Figure 5). The problems that occur in tropical areas in mapping rock alteration have been explained by (Siegal & Goetz 1977), where high vegetation density can be a limiting factor in the successful application of

Landsat series data for the detection and mapping of rock alteration due to hydrothermal processes.

In track 2, the ferrous oxide index pattern resembles track 1. The pattern that is formed is that the ferrous oxide index value rises at the edge of the oil and gas field and then falls inside the oil and gas field and at the northern border. Outside the field to the south, the ferrous iron oxide index value is 0.74, then rises at the edge of the oil and gas field to 1.60. The ferrous index value then fell again in the oil and gas field and to the north with an index value of 1.01. On track 3, on the southern border, the index value is 0.97 then gradually rises to 1.20 then falls again on the northern border to 0.88. The pattern formed on track 3 resembles the pattern on track 1. The ferrous oxide index at the edge of the oil and gas field is 1.34 then falls inside the oil and gas field rises again to the north of the oil and gas field with a value of 1.20 and falls again towards the outside of the oil and gas field next to north. The increase in ferrous oxide is also influenced by the combination of H₂S compounds with ferric oxide (limonite, hematite, and goethite (Fe₂O₃)) which forms ferrous oxide (Guo 1995). The ferrous oxide index map can be seen in Figure 5.

Constituents that may contain ferrous in thick sequences of sedimentary rock or red soil (redbed) are ilmenite (FeTiO₃), a solid solution of henite and hematite (x.FeTiO₃(I-X).Fe₂O) or intergrowth (two or more minerals that grow together and interlocking which generally occurs from simultaneous crystallization into two different minerals) of magnetite (Fe₃O₄) and clay minerals. Other forms of ferrous are siderite (FeCO), biotite, and greenalite (silicate mineral (SiO₂)) or iron ions that occur in the lattices of feldspars (Collinson 1968). Redbed bleaching occurs in areas where there is hydrocarbon seepage and changes ferric to ferrous and the red color disappears. The presence of pyrite due to hydrocarbon seepage can also occur due to the influence of hydrogen sulfate (Sun & Khan 2016):

The ferric oxide index value ranges from 0.95 – 3.55 with an average value of 1.79 and a standard



deviation of 0.21. In oil and gas fields, the ferric oxide index ranges from 1.12 – 2.49. At the edge of the oil and gas field in the southeast, which is an area

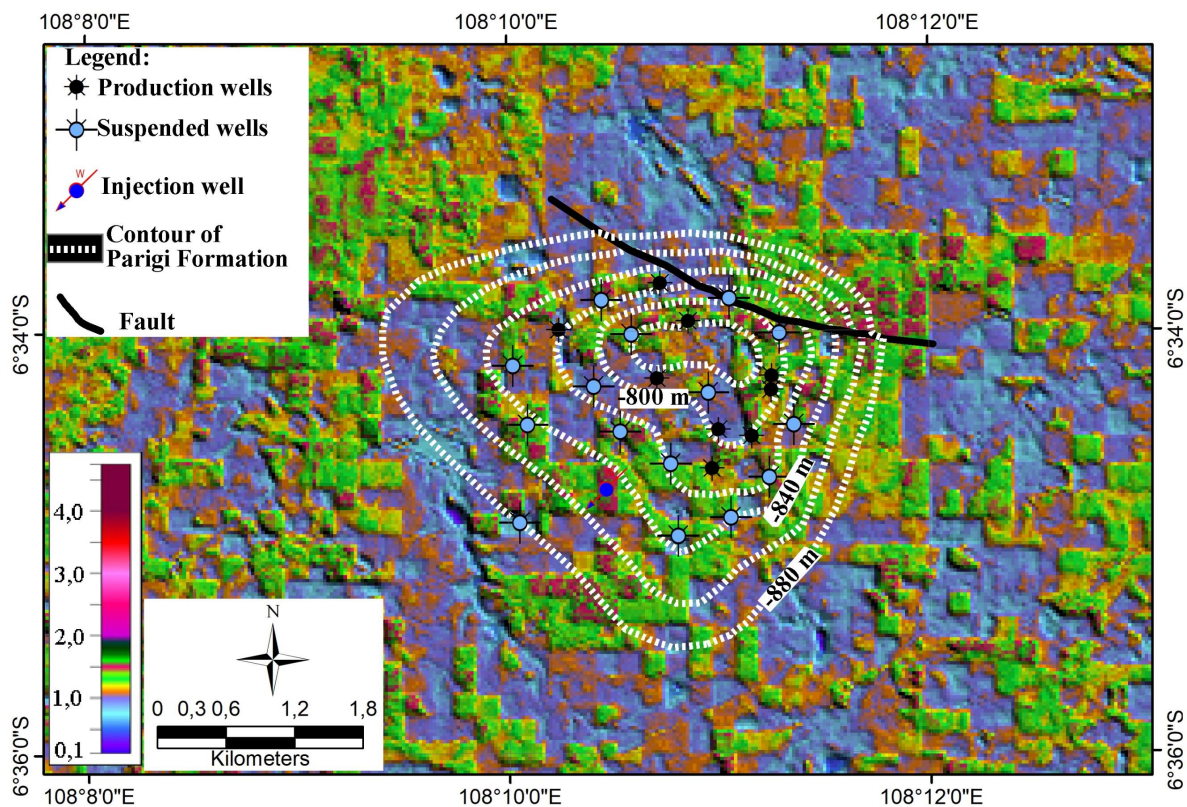


Figure 5
Ferrrous oxide index map on Landsat 8 OLI.

indicative of microseepage, there is a decrease in the value of the ferric oxide index. The results of the analysis of the ferrous oxide index and ferric oxide index showed that the ferric oxide index value was generally higher than the ferrous oxide index value. The ferric oxide index map can be seen in Figure 6.

A comparison of the pattern of ferric oxide index values with ferrous oxide shows the opposite pattern. Where if the ferric oxide index value increases, then the ferrous oxide index value decreases, conversely if the ferric oxide index value decreases, then the ferrous oxide index value increases.

Analysis of the ferric oxide index on 45 soil samples obtained from field surveys showed low values in the middle part of the oil and gas field and high at the edges. On track 1, outside the oil and gas field towards the west edge, it shows a high value, namely 2.11, which then drops to 1.48 and rises again in the middle of the field to 1.78. The index then fell near the edge of the oil and gas field to 1.38 and rose again towards the outside of the field to 2.13. Explained by (Hong 1999) due to the presence of oil and gas, ferric oxide values decreased in the middle

of the field and then increased outside the oil and gas field. Track 2 shows the same pattern as track 1, where on this track outside the oil and gas field the ferric oxide value is high with a value of 1.92, then decreases towards the edge of the field with a value of 1.42. The index value then rose again to 2.11 and around the southern edge to 1.38 then rose again in the middle of the field to 2.09. The ferric iron index value fell again on the eastern edge to 1.75 then rose again outside the oil and gas field to 2.10. Track 3 has a relatively similar pattern to track 1 and track 2. The consistent pattern of changes in vegetation, clay minerals, and iron oxide indicates that microseepage has occurred in the Tugu Barat field. This has been going on for a long time, causing changes on the land surface, both in vegetation and soil mineral concentrations (Noomen et al. 2012).

Iron Oxide Index on Soil Spectral

Ferrous and ferric oxide index analysis was carried out on soil spectra to increase the accuracy of the analysis on Landsat 8 OLI. Additional analysis was also carried out to sharpen the iron oxide index

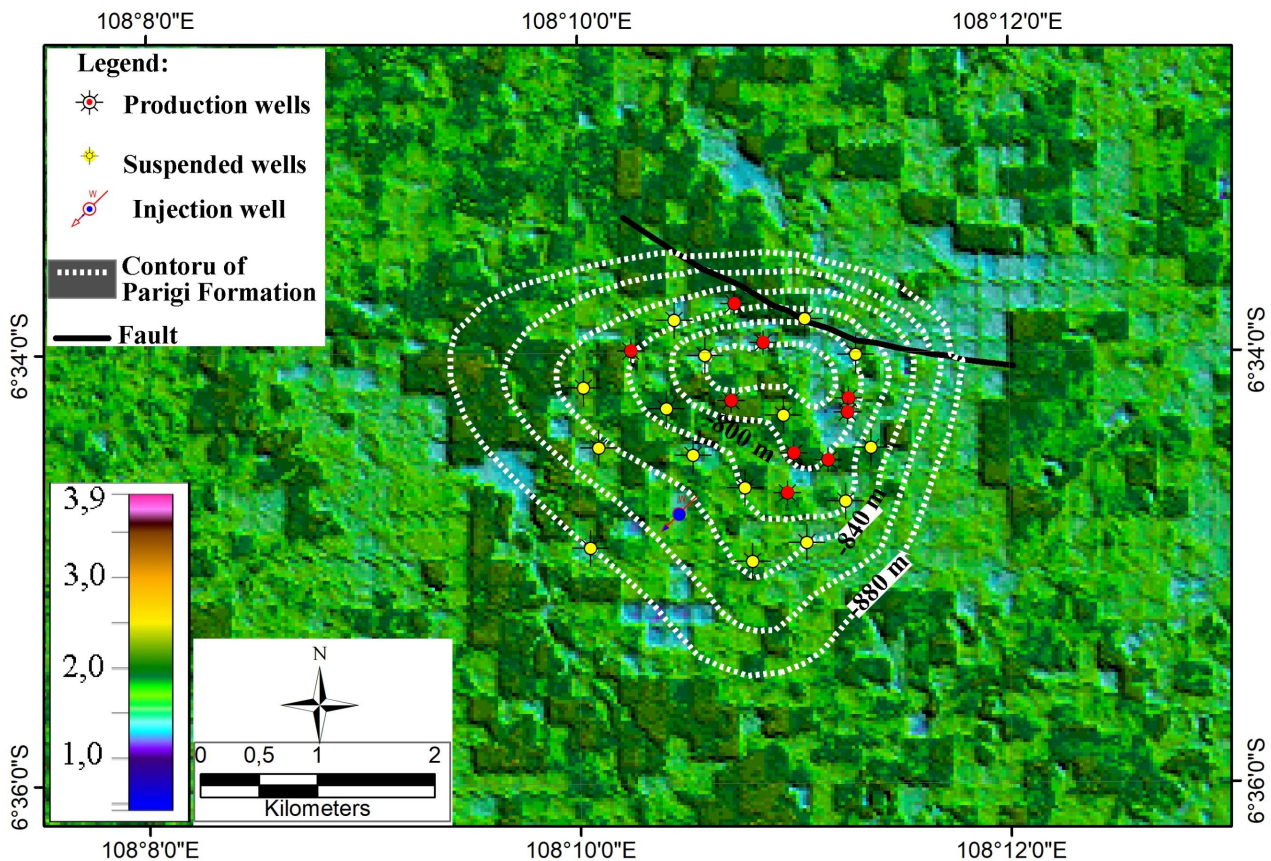


Figure 6
Ferric oxide index map on Landsat 8 OLI.

with NIODI. It is hoped that the results of this analysis can explain the anomaly in iron minerals due to microseepage. Ferrous is an iron atom that loses two electrons to form Fe^{+2} or written $Fe(II)$.

Analysis of the ferrous oxide index was carried out from soil reflectance spectral data recorded using ASD, which records soil spectra at close range to provide pure soil spectral values. Analysis of the ferrous oxide index on track 1 shows that it is low at the western edge of the field with a value of 0.81 and then tends to rise in the middle of the field with a value of 1.08. In general, the ferrous oxide index value in the center of the field is higher than at the edge of the oil and gas field (Figure 7a). The ferrous oxide index in path 2 is relatively uniform with an average value of 1.01. However, the northern edge of the field has the lowest value, namely 0.8 (Figure 7b). The ferrous oxide index value in track 3 is more volatile, going up and down like in track 1. The highest value in the oil and gas field is 1.08 and at the northern edge of the field, the lowest is 0.79 (Figure 7c).

The low ferrous oxide index condition is thought to be because ferrous ions generally dissolve easily and are oxidized to ferric ions. In the oxidation process, electrons are released, whereas ferrous ions, which are easily soluble, sometimes do not require oxygen and hydrogen (Mackereth et al. 1989). This condition occurs at neutral pH and the ferric ion will then form a precipitate and if it forms ferric hydroxide it becomes stable and does not dissolve easily. This is supported by the conditions at the time of the field survey which were still in the rainy season, so the soil conditions tended to still be damp/wet. The graph of the results of ferrous oxide index analysis on soil spectral results from ASD recording can be seen in Figure 7.

Analysis of the ferric oxide index from the ASD soil reflection spectra shows that at the western edge of the oil and gas field, it is low with a value of 1.31, then increases in the western interior with a value of 1.79 and decreases to the eastern edge with a value of 0.97. The pattern formed from analysis of the soil reflectance spectral ferric oxide index resembles the pattern formed in the Landsat 8 OLI ferric oxide index. The results of the soil reflectance spectral ferric oxide index on track 1 show that the area indicated is developing microseepage at sample points 14 – 21. The soil reflection spectral ferric oxide index on track 2 shows a pattern that resembles track 2 of the Landsat 8 OLI ferric oxide results.

The ferric oxide index was low at the southern edge of the field with a value of 1.19 then tended to rise inside the field with the highest value of 1.73 and fell again at the northern edge of the field with a value of 1.09. In path 3, the reflected spectral ferric oxide index results in relatively low index value changes. The ferric oxide index value on the southern edge tends to be low, namely 1.12, then rises inside the oil and gas field with the highest value of 1.46 and falls outside the oil and gas field with a value of 1.02. Based on the results of the ferric oxide index on Track 2 and Track 3, it is suspected that microseepage on the ground surface is more intensive in the south than in other places. The graph of the iron oxide index on 3 soil spectral survey lines can be seen in Figure 8.

Other analysis of soil reflectance spectra was carried out using the normalization of the iron oxide index (Normalized Fe Oxide Difference Index = NIODI). Positive values of NIODI indicate the presence of goethite and negative values indicate the presence of hematite. A value of zero indicates measurement uncertainty or that both minerals are present in the soil/rock (Viscarra Rossel et al. 2010).

The results of calculations using the NIODI formula at the research location obtained an average value of 0.008 and a standard deviation of 0.009. This shows that the NIODI value is relatively uniform. The highest NIODI value is 0.34 which is located on track 3 at sample point 41 and is located in the oil and gas field. Based on the NIODI results, it generally shows that at the research location, there is uncertainty regarding the presence of goethite and hematite minerals. This was proven by XRD analysis, where no goethite was found at 45 sample points, while hematite was found in small amounts at 15 sample points.

The results of the NIODI formula calculation on track 1 ranged from -0.011 to 0.023. The lowest NIODI values are located at the edge of the oil and gas field to the west and inside the oil and gas field, while the higher values are at the edge of the oil and gas field to the east. Low NIODI results, namely between -0.011 to 0.018, found hematite with concentrations of 1% to 4%. The NIODI calculation results at the study location are different from (Viscarra Rossel et al. 2010) even though Fe oxides play an important role in soil function. Fe oxides reflect the conditions of pH, redox potential, moisture, and temperature in the soil environment. The strong pigmenting effect of Fe oxides gives most soils their color, which is largely a reflection of the

soil's Fe mineralogy. Visible–near-infrared (vis–NIR), where hematite is found at values close to 0 (zero) positive and negative (Figure 9a).

The NIODI value on track 2 ranges from 0 to 0.012 with a standard deviation of 0.004. This result is low enough that it can be explained that at this location there is uncertainty regarding goethite. Further analysis showed that in the oil and gas fields from the north to outside the oil and gas fields, hematite was found with concentrations of 1% - 10%. This result is under path 1, where even though the NIODI value is not 0 (zero) but close to 0 (zero) hematite was found, but no goethite was found (Figure 9b). The NIODI value on track 3 ranges from

-0.010 to 0.034 with a standard deviation of 0.012. In this track, there is a higher NIODI value compared to paths 1 and 2, but it does not reflect the presence of goethite at the sample point based on XRD analysis (Figure 9c). Low (negative) NIODI values were found in hematite. Based on this NIODI analysis, it can be concluded that the NIODI value that is possible to contain hematite ranges from negative (-) to 0.018, and in general NIODI shows a low pattern in oil and gas fields.

Analysis of 45 sample points that have been carried out on Landsat 8 OLI/TIRS, soil reflectance spectra using the ferric oxide index, ferrous and NIODI shows changes in iron oxide concentration

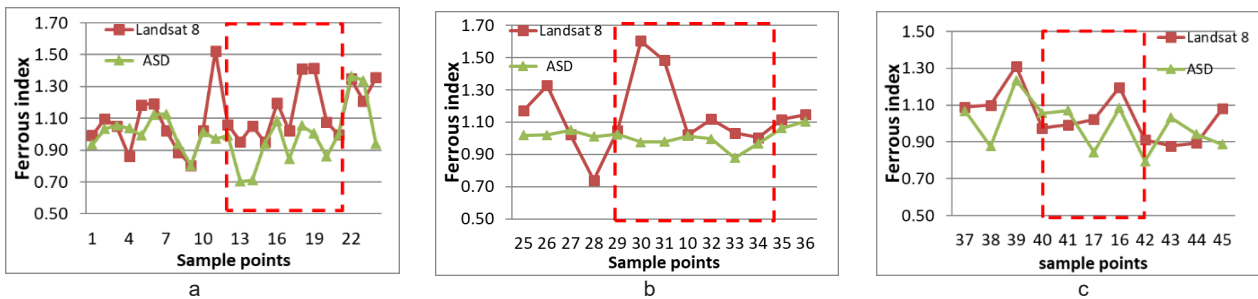


Figure 7

Ferrous oxide index graph from soil spectra recorded using ASD, (a) Survey path 1, (b) Survey path 2, and (c) Survey path 3.

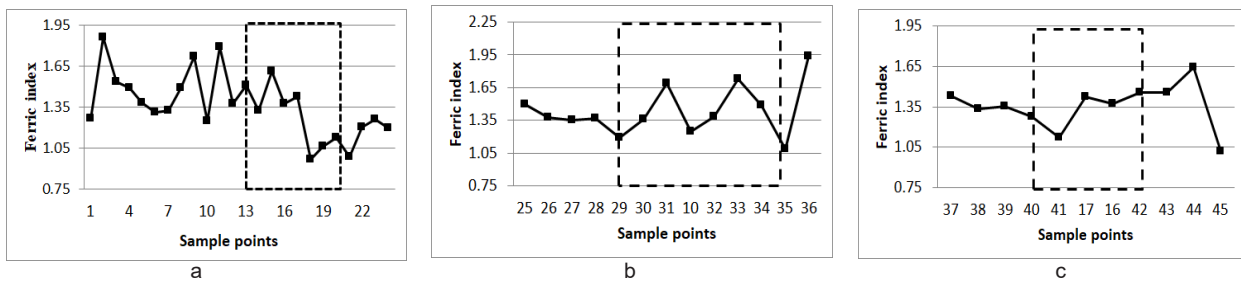


Figure 8

Graph of ferric oxide index from soil spectra on 3 field survey tracks, (a) Survey track 1, (b) Survey track 2, and (c) Survey track 3.

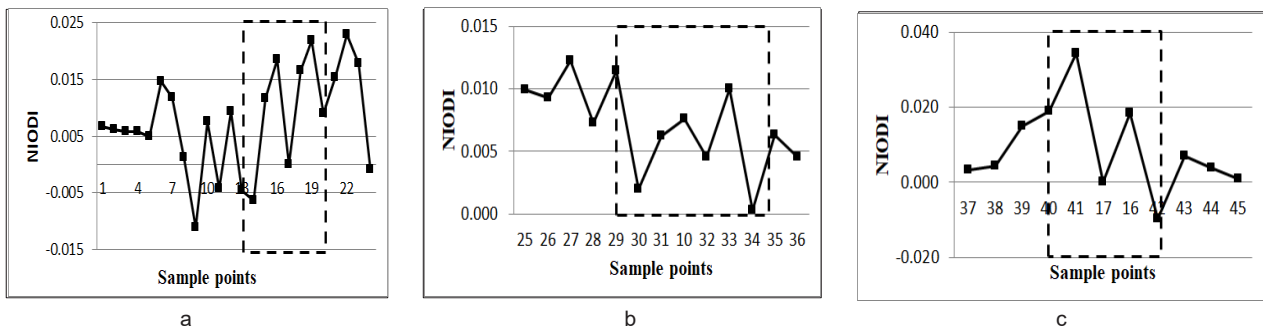


Figure 9

Graph of normalized iron oxide index (NIODI) values for 3 field survey routes, (a) survey route 1, (b) survey route 2, and (c) survey route 3.

between measurement/sampling points. However, these changes are not as clear as in the spatial analysis of both Landsat 8 OLI/TIRS and the spatial distribution of hematite concentrations resulting from XRD analysis.

Discussion

To obtain the best band combination for mapping hematite distribution, a band combination analysis was conducted using the best subsets regression (BSR) method with the integration of soil spectral data from ASD measurements and hematite concentration from XRD analysis. The results show that the mapping of hematite distribution can be done with the combination of bands B1, B2, B3, B4, and B5 with the coefficient of determination (R^2) is 0.71, R^2 (adjusted) is 0.67, the resulting algorithm for the mapping is as follows:

where H is distribution of hematite minerals, whereas B1, B2, B3, B4, and B5 are channels/canals/bands on Landsat 8 OLI.

$$H = 0,034 - 1,30B1 + 2,75B2 - 3,514B3 + 2,514B4 - 0,591B5 \quad (5)$$

The results of hematite distribution mapping show a pattern of high concentration at the top, then decreasing at the flanks and rising again at the edge of the oil and gas field structure (Figure 10). The pattern formed on the hematite distribution map successfully confirmed the existence of mineral alteration which indicated the presence of microseepage. This alteration occurs in almost all oil and gas fields due to the effect of gas diffusion from the reservoir, even though there are caps that are considered impenetrable (Schumacher 2001; Van Der Meer et al. 2002), and there are chimneys (Saunders et al. 1999; Schumacher 1996; van der Werff et al. 2007) The patterns formed in mineral alteration also confirm the concepts explained by (Hong 1999); (Saunders et al. 1999); and (Schumacher 1996).

The hematite concentration resulting from the XRD analysis is under the NIODI analysis where negative (-) to near zero (zero) values are an indication of the presence of hematite (Viscarra Rossel et al. 2010) even though Fe oxides play an important role in soil function. Fe oxides reflect the conditions of pH, redox potential, moisture, and temperature in the soil environment. The strong pigmentation effect of Fe oxides gives most soils their color, which is largely a reflection of the soil's Fe mineralogy. Visible–near-infrared (vis–NIR). In this

study, soil samples that were detected to contain hematite were in the NIODI value range from negative (-) to 0.018. Explained by (Petrovic et al. (2012) that areas that experienced bleaching due to seepage had lower hematite concentrations compared to areas that did not experience bleaching. The process that occurs at this location is that hematite is reduced and it has turned into pyrite. Based on the distribution pattern of hematite, it can be concluded that the presence of microseepage at the edge of the field is more intensive. This confirms the existence of microseepages inferred from vegetation and clay mineral analysis (Susantoro et al. 2020).

The presence of intensive alteration forming clay and iron oxide indicates that there are micro seepages and passive seepages characterized by bleaching effects which have the opportunity to support oil and gas exploration (Habib et al. 2019). Field surveys observed that the red soil outside the oil and gas field did not experience bleaching, it is suspected that the iron oxide content at this location was relatively high. XRD analysis of soil samples located at the edge of the field shows that the hematite concentration is relatively low, then towards the center of the field/top of the structure the hematite concentration increases, but is still lower than outside the field. This shows the existence of a series of other mineralogical and geochemical indicators, especially the partial bleaching process of red soil due to micro-seepage. (Asadzadeh & de Souza Filho 2020). This has been explained by (Petrovic et al. 2008, 2012); and (van der Meer et al. 2000) that long-term oil and gas seepage can result in changes/alteration of rocks and soil. This indication has the opportunity to be used to support oil and gas exploration activities in Indonesia by further studying micro-seepage in existing oil and gas fields. The results can be applied to assess leads and prospects, whether there are micro-seepages that can be used as a sign of oil and gas trapped in the reservoir.

CONCLUSION

Research on the distribution of iron oxide in the surface soil of oil and gas fields found a subtle anomaly in hematite concentration, where it was low at the edges then tended to increase at the top/middle, but this pattern was not so clear because of the presence of red soil with high hematite content located to the north. field. This area is geographically at a lower elevation. Ferrous oxide concentrations based on Landsat 8 OLI show an increase at the

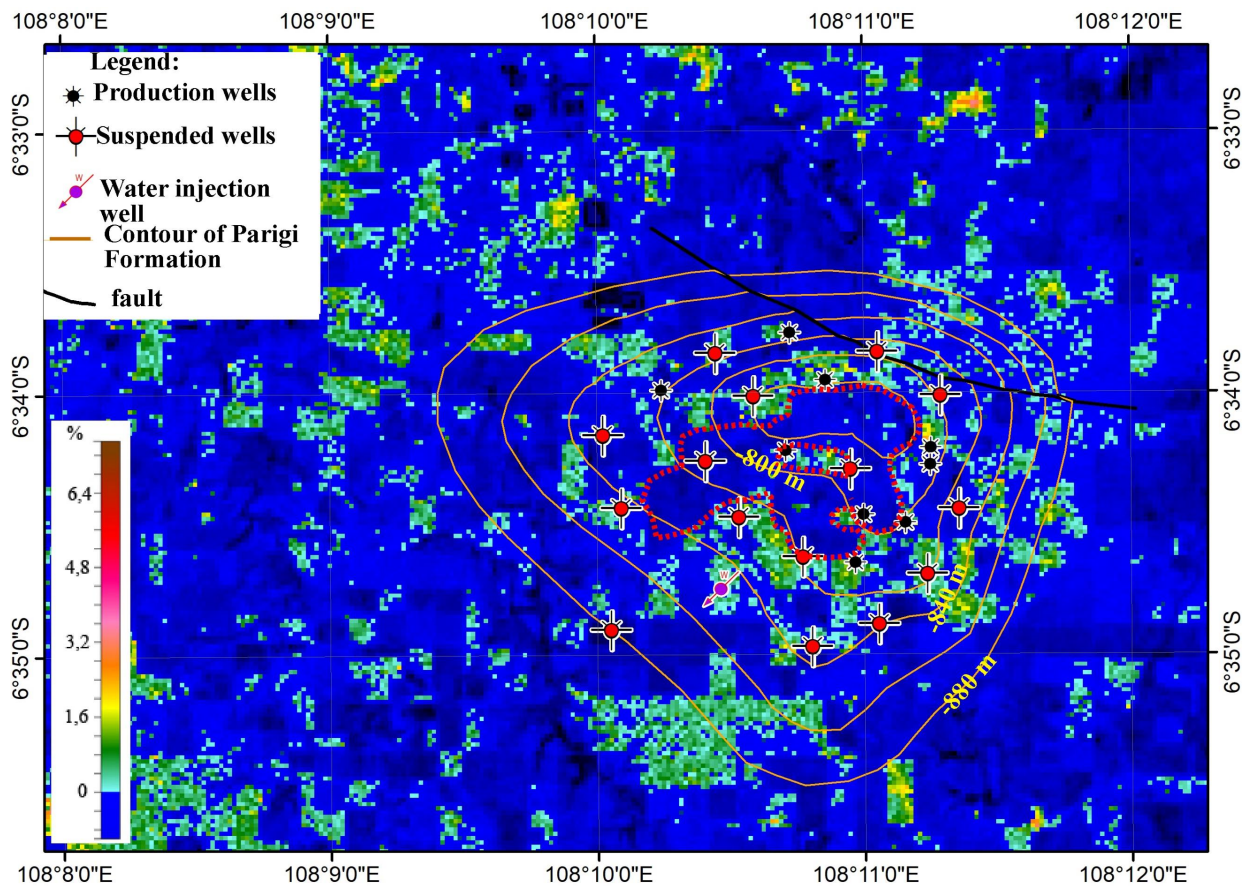


Figure 10
Hematite mineral distribution map resulting from modeling of soil reflectance spectral and mineral concentration applied to Landsat 8 OLI.

edges of oil and gas fields, especially in the southeast. On the west side of the field, this condition is somewhat difficult to see because of the high density of vegetation. Ferric oxide concentrations showed the opposite pattern to ferrous iron concentrations. Where if the ferric oxide index value increases, the ferrous oxide index value decreases, conversely, if the ferric oxide index value decreases, the ferrous oxide index value increases. These results are supported by the ferrous oxide index results from soil reflectance spectra recorded using ASD. Where the concentration of ferrous oxide is low at the edge of the oil and gas field then tends to rise in the middle of the oil and gas field. Analysis of ferric oxide from soil reflectance spectra from ASD results does not show clear differences but has a pattern similar to the Landsat 8 OLI ferric oxide index. NIODI analysis shows that no goetite has been identified in the Tugu Barat oil and gas field, but small amounts of hematite have been identified. Based on hematite concentration and spectral reflectance, hematite mapping was carried out in the Tugu Barat field using

bands B1, B2, B3, B4, and B5 with a coefficient of determination (R^2) of 0.71, R^2 (adjusted) of 0.67. The results show that the hematite concentration at the top of the anticline is high, then decreases and rises again at the edge of the oil and gas field structure. This pattern indicates hematite alteration in oil and gas fields due to micro-seepage. Based on these results, we conclude that in the West Tugu field, there are indications of micro-seepage, especially on the southeastern edge. This study can be used as a consideration for selecting leads and prospects to determine the continuation of exploration.

ACKNOWLEDGMENT

The authors would like to thank the National Research and Innovation Agency (BRIN) and Research for Advanced Indonesia (RIIM), the Faculty of Earth Science and Technology-Bandung Institute of Technology, the Geoinformatics Research Center-OREI, the Geological Survey Center-Geological Agency and the R&D Center for Oil

and Gas Technology LEMIGAS-Ministry of Energy and Mineral Resources, which has supported the research. The authors would also like to thank PT Pertamina PHE Upstream Technology for facilitating this research and all related parties who assisted in field surveys, and laboratory analysis and provided suggestions for completing this research.

Fundings

The Advanced Indonesia Research and Innovation RIIM funded this research with grant numbers 82/II.7/HK/2022. This research is also supported by the Faculty of Earth Sciences and Technology-Bandung Institute of Technology and PT Pertamina Upstream Technology.

GLOSSARY OF TERMS

Symbol	Definition	Unit
ASD	Analytic Spectral Device	
Fe+2 = FE(II)	Ferrous	
Fe+3 = FE (III)	Ferric	
Landsat 8 OLI	Land Satellite 8 Operational Land Imager	
Landsat TM	Land Satellite Thematic Mapper	
NIODI	Normalized Iron Oxide Difference Index	
NIR	Near Infra-Red	
pH	Potential of Hydrogen	
RMSE	The Root Mean Squared Erro	
XRD	X-Ray diffraction	

REFERENCES

- Annisa, W. & Purwanto, B., 2010, Retensi P oleh Oksida Besi di Tanah Sulfat Masam setelah Reklamasi Lahan. *Jurnal Sumber Daya Lahan* 4, 47–56.
- Asadzadeh, S. & de Souza Filho, C.R., 2020, Characterization of microseepage-induced diagenetic changes in the Upper-Red Formation, Qom region, Iran. Part I: Outcrop, geochemical, and remote sensing studies. *Marine and Petroleum Geology* 117, 104149. <https://doi.org/10.1016/j.marpetgeo.2019.104149>.
- Bergstresser, M., 2018, Difference Between Ferric Oxide & Ferrous Oxide, in: *Organic and Inorganic Compounds Study Guide*.
- Collinson, D., 1968, Ferrous and Ferric Iron in Red Sediments and Their Magnetic Properties. *Geophys. J.R. Astr. Soc* 16, 531–542. <https://doi.org/10.1111/j.1365-246X.1968.tb02313.x>.
- Crystiana, I., Susantoro, T.M. & Firdaus, N., 2015, Pengolahan Data Citra Satelit untuk Mengidentifikasi Potensi Jebakan dalam Kegiatan Eksplorasi Migas. *Lembaran Publikasi Minyak dan Gas Bumi* 49, 41–51.
- Crystiana, I., Susantoro, T.M. & Junaedi, T., 2014, Identifikasi potensi migas melalui citra satelit dengan pendekatan anomali topografi (Studi kasus daerah Indramayu dan sekitarnya. *Lembaran Publikasi Minyak dan Gas Bumi* 48, 89–102.
- Drury, S., 1987, *Image Interpretation in Geology*. Allen and Unwin, London.
- Guo, D., 1995, Direct Searching for Oil and Gas by Remote Sensing Technology. *Acta Petrolei Sinica* 16, 9–16.
- Habib, A., Abuzar, M.K., Ahmad, I., Shakir, U., Mahmood, S.A., Khan, M.A. & Mahmood, M.F., 2019, Detection of mineral alteration induced by hydrocarbon microseepages by using remotely sensed data in the Fateh Jang area of the Northern Potwar region of Pakistan. *Arabian Journal of Geosciences* 12, 121. <https://doi.org/10.1007/s12517-019-4225-3>.
- Hidayat, A., Hardjowigeno, S., Soekardi, M. & Sabiham, S., 2002, Peranan Oksida Besi terhadap Sifat Tanah Berpelapukan Lanjut. *Jurnal Tanah dan Iklim* 20, 47–56.
- Hong, Y., 1999, *Imaging spectrometry for hydrocarbon microseepage*. ITC Dissertation. International Institute for Geo-Information Science and Earth Observation, Netherlands.
- Hunt, G. & Salisbury, J., 1976, Visible and Near Infrared Spectra of Minerals and Rocks: XI. Sedimentary Rocks. *Modern Geology* 5, 211–217.
- Hunt, G., Salisbury, J. & Lenhoff, C., 1974, Visible and Near Infrared Spectra of Minerals and Rocks: IX. Basic and Ultrabasic Igneous Rocks. *Modern Geology* 5, 15–22.

- Liu, X., Bloemendal, J. & Rolph, T., 1994, Pedogenesis and Paleoclimate Interpretations of Magnetic Susceptibility Record of Chinese Loess-Paleosol Sequences. *Geology* 22.
- Mackereth, F.J., Heron, J. & Talling, J., 1989, *Water Analysis*. Fresh-Water Biological Association, Cumbria, UK.
- Maher, B. & Thompson, R., 1992, Paleoclimate Significance of Mineral Magnetic of The Chinese Loess and Paleosols. *Quaternary Research*. C.
- Noomen, M.F., van der Werff, H.M.A. & van der Meer, F., 2012, Spectral and spatial indicators of botanical changes caused by long-term hydrocarbon seepage. *Ecological Informatics* 8, 55–64. <https://doi.org/10.1016/j.ecoinf.2012.01.001>.
- Ouattara, T., Couture, R., Bobrowsky, P. & More, A., 2004, *Remote Sensing and Geosciences*. Geological Survey of Canada, Ottawa.
- Petrovic, A., Khan, S.D. & Chafetz, H.S., 2008, Remote Detection and Geochemical Studies for Finding Hydrocarbon-Induced Alterations in Lisbon Valley, Utah. *Marine and Petroleum Geology* 25, 696–705. <https://doi.org/10.1016/j.marpetgeo.2008.03.008>.
- Petrovic, A., Khan, S.D. & Thurmond, A.K., 2012, Integrated hyperspectral remote sensing , geochemical and isotopic studies for understanding hydrocarbon-induced rock alterations. *Journal Marine and Petroleum Geology* 35, 292–308. <https://doi.org/10.1016/j.marpetgeo.2012.01.004>.
- Rajesh, H., 2004, Application of Remote Sensing and GIS in Mineral Resource Mapping- An Overview. *Journal of Mineralogical and Petrological Sciences* 99, 83–103.
- Salati, S., 2014, Characterization and Remote Sensing of Onshore Hydrocarbon Seep-Induced Alteration. University of Twente, ITC. <https://doi.org/10.3990/1.9789036536295>
- Saunders, D.F., Burson, R.K. & Thompson, C.K., 1999, Model for Hydrocarbon Microseepages and Related Near-Surface Alteration. *Bull. Am. Ass. Petrol. Geology* 83, 170–185.
- Schumacher, D., 2001, Petroleum Exploration in Environmentally Sensitive Areas: Opportunities for Non-Invasive Geochemical and Remote Sensing Methods, in: Rock the Foundation Convention. Canadian Society of Petroleum Geologists, Canada, pp. 012-1-012–5.
- Schumacher, D., 1996, Hydrocarbon-induced alteration of soils and sediments, in: Schumacher, D., A.A.M. (Eds.), *AAPG Memoir*. The American Association of Petroleum Geologists, pp. 71–89. <https://doi.org/10.1306/m66606c6>.
- Schwertmann, U. & Taylor, R., 1989, Iron Oxides, in: Dixon, J., Weed, S. (Eds.), *Mineral in Soil Environments*. Soil Science Society of America, Wisconsin, USA.
- Shi, P., Fu, B. & Ninomiya, Y., 2010, Mapping Hydrocarbon Seepage-Induced Anomalies In The Arid Region, West China Using Multispectral Remote Sensing. *International Archives of the Photogrammetry, Remote Sensing and Spatial Information Science XXXVIII*, 442–447.
- Siegel, B. & Goetz, A.F.H., 1977, Effect of Vegetation on Rock and Soil Discrimination. *Photogrammetric Engineering and Remote Sensing* 43, 191–196.
- Suliantara, S., Susantoro, T.M., Setiawan, H.L. & Firdaus, N., 2021, A preliminary study on heavy oil location in Central Sumatra using remote sensing and geographic information system. *Scientific Contributions Oil and Gas (SCOG)* 44, 39–54. <https://doi.org/10.29017/SCOG.44.1.489>.
- Sun, L. & Khan, S., 2016, Ground-Based Hyperspectral Remote Sensing of Hydrocarbon-Induced Rock Alterations at Cement , Oklahoma. *Marine and Petroleum Geology* 77, 1243–1253. <https://doi.org/10.1016/j.marpetgeo.2016.08.019>.
- Susantoro, T.M., Saepuloh, A., Wikantika, K. & Maryanto, A., 2024, Hydrocarbon Seepage Analysis on a Hydrocarbon Field in Indonesia Based on Plant Stress Using Landsat-8 Operational Land Imager and Field Measurements Hydrocarbon Seepage Analysis on a Hydrocarbon Field in Indonesia Based on Plant Stress Using Landsat-8 Op. *EVERGREEN Joint Journal of Novel Carbon Resource Sciences & Green Asia Strategy* 11, 756–770. <https://doi.org/10.5109/7183356>.
- Susantoro, T.M., Saepuloh, A., Agustin, F., Wikantika, K. & Harsolumakso, A.H., 2020, Clay mineral

- alteration in oil and gas fields: integrated analyses of surface expression, soil spectra, and X-ray diffraction data. *Canadian Journal of Remote Sensing* 46, 237–251. <https://doi.org/10.1080/07038992.2020.1771174>.
- Susantoro, T.M., Suliantara, Harto, A.B., Setiawan, H.L., Nugroho, G., Candra, D.S., Jayati, A., Sulma, S., Khomarudin, M.R., Arief, R., Maryanto, A., Hestrio, Y.F. & Kurdianto, 2023a, The Potential of Remote Sensing Data for Oil And Gas Exploration in Indonesia: a Review. *Scientific Contributions Oil and Gas* 46, 29–43. <https://doi.org/10.29017/SCOG.46.1.1346>.
- Susantoro, T.M., Suliantara, S., Setiawan, H.L. & Wikantika, K., 2023b, Study of earth surface morphological anomalies based on Landsat OLI 8 data and soil grain size in oil and gas field in undulating morphology, in: *The 9th International Seminar on Aerospace Science and Technology (ISAST 2022)*. AIP Publishing, Jakarta, Indonesia, pp. 1–10. <https://doi.org/10.1063/5.0181459>.
- Susantoro, T.M., Wikantika, K., Harto, A.B. & Suwardi, D., 2019, Monitoring sugarcane growth phases based on satellite image analysis (A case study in indramayu and its surrounding, West Java, Indonesia). *HAYATI Journal of Biosciences* 26, 117–128. <https://doi.org/10.4308/hjb.26.3.117>.
- Susantoro, T.M., Wikantika, K., Saepuloh, A. & Harsolumakso, A.H., 2018, Selection of vegetation indices for mapping the sugarcane condition around the oil and gas field of North West Java Basin, Indonesia. *{IOP} Conference Series: Earth and Environmental Science* 149, 12001. <https://doi.org/10.1088/1755-1315/149/1/012001>.
- Van der Meer, F., Dijk, P., Kroonenberg, S., Hong, Y. & Lang, H., 2000, Hyperspectral Hydrocarbon Microseepage Detection and Monitoring: Potentials and Limitations, in: *The 2nd EARSeL Workshop on Imaging Spectroscopy, 11-13 July 2000*. ITC, Enschede, The Netherlands., pp. 1–9.
- Van Der Meer, F., Van Dijk, P., van der Werff, H.M.A. & Hong, Y., 2002, Remote sensing and petroleum seepage: a review and case study. *Terra Nova* 14, 1–17. <https://doi.org/10.1046/j.1365-3121.2002.00390.x>.
- Van der Werff, H.M.A., Noomen, M.F., Van Der Meijde, M. & van der Meer, F., 2007, Remote sensing of onshore hydrocarbon seepage: Problems and solutions, in: Teeuw, R.M. (Ed.), *Mapping Hazardous Terrain Using Remote Sensing*. London Geology Society, London, pp. 125–133. <https://doi.org/10.1144/SP283.11>.
- Viscarra Rossel, R.A., Bui, E.N., De Caritat, P. & McKenzie, N.J., 2010, Mapping iron oxides and the color of Australian soil using visible-near-infrared reflectance spectra. *Journal of Geophysical Research: Earth Surface* 115, 1–13. <https://doi.org/10.1029/2009JF001645>.